ADVANCED FUNCTIONAL MATERIALS
www.afm-journal.de

Superspreading of Polyelectrolyte Complex Solution for Constructing Hydrogel Coatings on Diverse Substrates

Congying Wei, Chuangqi Zhao, Yunfei Ru, Yingzhi Sun, Tianyi Zhao, Shuanhu Qi, Jiajia Zhou,* and Mingjie Liu**

Injectable hydrogels have emerged as versatile materials with potential applications in various fields, including biomedicine, lubrication, adhesion, surface coatings, and tissue engineering. However, the critical aspect of spreading and wetting on various substrates, which is essential for obtaining significant interfacial properties, has not been adequately addressed. This work presents an approach to prepare hydrogel coatings on kinds of substrates through the superspreading of polyelectrolyte complex solution during its liquid-liquid phase inversion process. Due to the low interfacial tension, the solution spreads and wets various surfaces underwater driven by osmotic pressure, improving the contact area and interface integration. Combined with the simultaneous sol-gel transition through electrostatic interaction, it forms a stable and homogeneous hydrogel coating. The hydrogel coating possesses control thickness (4–8 µm), improved hydrophilicity (CA decrease from 102° to 10°), interfacial toughness (increase from 70 to 455 J m^{-2}), and lubrication performance (coefficients of friction decrease from 0.712 to 0.112). The work provides an excellent opportunity to investigate the spreadability and wettability in a water/water/solid three-phase system and develop functional hydrogel coatings for various applications.

1. Introduction

Injectable hydrogel formulations are especially attractive due to their excellent biocompatibility, high permeability, flexibility in fabrication, desirable physical properties, and minimally invasive delivery procedures.[1] The use of injectable hydrogels is particularly advantageous in applications where the final form and shape are either irrelevant or determined by the void or space into which they are injected.[2] Injectable hydrogels have shown high potential for biomedical applications such as drug delivery, tissue engineering, and regenerative medicine.[3–5] The most common in situ gelation strategies rely on either chemical or physical crosslinking. Compared to chemical crosslinking hydrogels (photoirradiation and self-reactive reactions), physical hydrogels formed through a reversible phase transition in response to environmental conditions (e.g., temperature, pH, and ionic strength) avoid the biocompatibility problems of residual initiators or monomers.[6–9] Recently, physically injectable hydrogels based on water solvents have attracted considerable attention because of the harmful nature of their counterparts organic solvents.[10] The presence of water or aqueous solutions also endows injectable hydrogels with the ability to carry hydrophilic therapeutic agents and controlled release for treating diseases or mimicking structures of the extracellular matrix (ECM) and tissues.[11,12]

To be successful, injectable hydrogels should have a large viscosity to avoid mixing in water during underwater injection. Furthermore, gels should be formed in a short time to prevent undesired leakage of agents or migration to unintended sites.[13] Kim et al. reported injectable hydrogels using spontaneous gelation mechanisms based on covalent bonding and noncovalent interactions during injection through a dual syringe.[14] Liu et al. and Zhao et al. developed injectable hydrogels on the basis of hydrophobic molecules and interactions that could displace water molecules on the surface. These hydrogels showed impressive results in wound hemostasis and sealant applications.[15,16] In order to render hydrogels insoluble in water, they possess significant viscosity, often in an entangled state with long polymer chains exhibiting restricted mobility. External pressure, applied through a surgical spatula, becomes necessary to augment the contact area.[14,17] The underlying mechanisms of interfacial

C. Wei, Y. Ru, Y. Sun, T. Zhao, M. Liu
Key Laboratory of Bioinspired Smart Interfacial Science and Technology of Ministry of Education
School of Chemistry
Beihang University
Beijing 100191, P. R. China
E-mail: liumj@buaa.edu.cn

C. Zhao
University of Science and Technology of China
Hefei 230026, P. R. China

C. Zhao
Suzhou Institute for Advanced Research
University of Science and Technology of China
Suzhou 215123, China

S. Qi
School of Physics
Beihang University
Beijing 100191, P. R. China
E-mail: qishuanhu@buaa.edu.cn

J. Zhou
South China Advanced Institute for Soft Matter Science and Technology
School of Emergent Soft Matter and Guangdong Provincial Key Laboratory of Functional and Intelligent Hybrid Materials and Devices
South China University of Technology
Guangzhou 510640, P. R. China
E-mail: zhouj2@scut.edu.cn

The ORCID identification number(s) for the author(s) of this article can be found under https://doi.org/10.1002/adfm.202400581

DOI: 10.1002/adfm.202400581

adhesion mostly focus on covalent or noncovalent crosslinking with tissue surfaces,[18] while the spreading and wetting of hydrogels on the surface are often overlooked, which is a primary prerequisite for successful adhesion.

Wetting and spreading are fundamental interface phenomena that play a crucial role in various applications, including oil extraction, waterproofing, adhesion, and coating, which have mainly focused on gas/liquid/solid three-phase interfaces.[19,20] In the past, multilayer coatings are primarily constructed using chemical interactions and bonding, such as covalent bonding, hydrogen bonding, and host-guest interactions.[21] However, these coatings face limitations concerning chemical modification, regulation of micro/nanostructures, and compatibility between hydrophilic and hydrophobic substrates.[22] Additionally, applying coatings to complex geometrically shaped substrates has proven to be challenging.[23] Moreover, the simultaneous introduction of small molecules, unreacted monomers, or the diffusion of initiators can lead to poor biocompatibility, rendering such coatings unsuitable for biomedical applications.[22] Therefore, there is a need for novel strategies to address these challenges to enhance the performance and expand potential applications of wetting, spreading, and coating technologies.

The spreading and wetting of liquids on solid surfaces play a crucial role in establishing the foundation for subsequent chemical bonding. In this work, we developed a general strategy combined with the motion and crosslinking of polymer chains to realize the superspreading of polyelectrolyte complex solutions on a wide range of surfaces, including metals, polymers, and glass in a water/water/solid tri-phase system. The lower interfacial tension of the solution allows it to replace the water film in front of the substrate, potentially leading to complete spreading and wetting. With the subsequent progress of the sol-gel transition, a superheating-mediated hydrogel could be successfully coated onto various substrates. The resulting coatings exhibit controllable thickness (4–8 μm), enhanced wettability (CA≈10.0° on PDMS), and reasonable lubrication effects (coefficients of friction = 0.112 ± 0.003).

It is important to note that this strategy enables superspreading of most oppositely charged polyelectrolytes, allowing for the selection of materials with relevant functionalities. Additionally, this approach expands the selection of compatible substrates and achieves wettability matching between solutions and substrates, especially for hydrophobic surfaces, without the need for post-modification. The resulting coatings, with their inherent simplicity in fabrication, hold tremendous potential for various applications, including biomedical implants, electrochemical devices, and surface protection.[24] Our findings offer valuable insights into the design of advanced hydrogel coatings and provide a foundation for the development of diverse functional and interface materials.

2. Results and Discussion

2.1. The Liquid-Liquid Phase Inversion Strategy

The liquid-liquid phase inversion strategy relies on electrostatic interactions between polyelectrolytes. In aqueous solutions, polyelectrolyte complexes (PECs) are formed by oppositely charged polyelectrolytes through electrostatic interactions[25,26] (**Figure 1a**). Intermolecular association between opposite charges is also controlled by salt concentration. Upon the addition of salt, the ion pair dissociates and each salt ion pairs with a polyelectrolyte segment of opposite charge, lowering the cross-linking among polyelectrolytes. At higher salt concentrations, crosslinking significantly decreases, transforming "intrinsic" charge compensation to "extrinsic" and eventually separating polyelectrolyte chains from each other completely[27,28] (Figure 1b). When PEC solution is dialyzed in water or a lower salt concentration solution, the salt and counterions of PEC diffuse out the system by osmotic pressure, causing polyelectrolyte chains to be crosslinked again and produce tough physical hydrogels[29,30] (Figure 1c). Schlenoff et al. studied the association process of polyelectrolytes spanning from complexes (solid) to coacervates (elastic liquid) to dissolved solutions with increasing [KBr].[31] On the basis of this reversible ionic bond, Gong[32] and Zheng et al.[33] exploited the processability of the PEC to produce high-performance fibers, sheets, and films. Kamperman et al. developed polyelectrolytes triggered by temperature and ionic strength for multi-responsive coacervate adhesion.[34] However, the investigation of this strategy to achieve superspreading and super wetting on wet surfaces has yet to be conducted.

2.2. Preparation of the Injectable Hydrogel

In this work, the injectable hydrogel is composed of oppositely charged polyelectrolytes, chitosan quaternary ammonium salt (QCS), and carboxymethylcellulose sodium (CMCNa) (**Figure 2a**). As shown in Figure 2b, the QCS-CMCNa complex was obtained by mixing a QCS aqueous solution (1.0 mL; 10 mg mL^{-1}) with a CMCNa aqueous solution (1.0 mL; 10 mg mL^{-1}) with a charge ratio of 1:1. Liquid-solid phase separation occurs immediately, and settling yielded a white precipitate phase (Figure 2c). Electrostatic complexation between the carboxylates and azetinidium groups is responsible for chain aggregation.[35] Adding to a concentrated NaCl solution allows the transition of the associated QCS-CMCNa complex from coacervate to dissolved solutions (Figure S1, Supporting Information). Figure 2d shows the phase diagram of the QCS-CMCNa polymer concentration versus salt concentration. The pink, blue, and green regions represent the precipitate, coacervation, and solution phases, respectively. Compared to the precipitate, the coacervate can be temporarily stable and has a certain degree of fluidity (Figure S2a, Supporting Information). The borderline between the solution (green) and coacervate (blue) phases defined the critical NaCl concentration (C_{NaCl}) that triggers the dissociation of the QCS-CMCNa complex to solution as supported by their turbidity curves (Figure S2b,c. Supporting Information). The C_{NaCl} increased as the polymer concentration increased. For example, at a polymer concentration of 15%, the coacervation phase was observed from QCS-CMCNa$_{0.4\ M}$ to QCS-CMCNa$_{0.6\ M}$ (subscripts show the [NaCl] in the dilute phase). A homogeneous solution was observed from QCS-CMCNa$_{0.7\ M}$ to QCS-CMCNa$_{5\ M}$ (Figure 2e; Figure S3, Supporting Information). The function of added salt is to pair with polyelectrolytes and break their crosslinks, leading to a decrease in the viscosity of the solution at high salt concentration.[32]

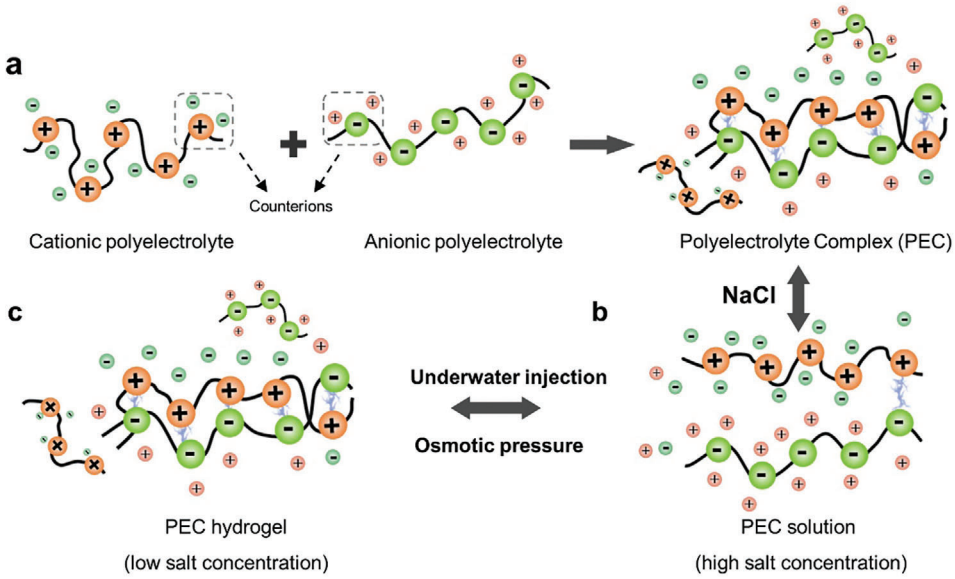

Figure 1. Schematic illustration of the reprocessing of PECs. a) PECs are prepared by mixing cationic polyelectrolyte and anionic polyelectrolyte solutions. b) On the basis of the ionic shielding effect, PEC solutions could be prepared by dissolving in concentrated NaCl solution. c) Driven by the osmotic pressure, polyelectrolyte chains are crosslinked again to produce tough physical hydrogels by being injected into the lower NaCl concentration.

2.3. The Liquid-Liquid Phase Inversion of Injectable Hydrogel

Once the QCS-CMCNa precursor solution is injected underwater, salt co-ions would diffuse to the water due to concentration gradient, allowing oppositely charged polyelectrolytes to reform multiple ionic bonds. The viscous polymer solution transforms to a nonflowable gel state and undergoes the liquid-liquid phase inversion process.[13] The gelation times of different NaCl concentrations were evaluated using dynamic time sweep rheological experiments, as evidenced by the crossover of storage modulus (G′) and loss modulus (G″). At NaCl concentrations of 0.7–0.9 M, a fraction of crosslinked points in the precursor solution was retained, resulting in high solution viscosity and weak chain moving ability (stronger hydrodynamic friction), which experienced ≈1 min gelation time (Figure 2f). When adding salt concentrations to 1–5 M, the majority of ionic pairs were broken and residual crosslinks were reduced, resulting in low viscosity of the precursor solution and longer gelation times, i.e., 3–15 min (Figure 2g).

The liquid-liquid phase inversion process is not only related to the viscosity of solutions but also to the diffusion of counterions. Along this direction, the ion type should be an essentially important factor in the ion−polyelectrolyte interaction. The specific ion effect is further investigated by choosing the series of alkali ions-LiCl, NaCl, and KCl salt.[36] First, during the dissociation process of PEC to PEC solution (Figure 1b), the critical NaCl concentration (C_{NaCl}) will be affected by ion−polyelectrolyte interaction. As shown in **Figure 3**a,b, the obtained QCS-CMCNa solution in alkali ions has an order of $C_{KCl} < C_{NaCl} < C_{LiCl}$. When the polymer concentration is 15%, the solution viscosity is $\eta_{KCl} < \eta_{NaCl} < \eta_{LiCl}$ (Figure 3c), demonstrating that the stronger interaction between counterions and polyelectrolytes reduces the degree of crosslinking of polymer molecular chain, leading to a lower critical concentration and solution viscosity.

The difference in ion−polyelectrolyte interaction be attributed to the difference in ions hydration ability. For instance, the molar Gibbs energy of hydration is 475 kJ mol^{-1} for Li^+, 430 kJ mol^{-1} for Na^+, and 295 kJ mol^{-1} for K^+.[37] This sequence highlights the order of binding strength order between ions and water as $Li^+ > Na^+ > K^+$, inversely related to ion-polyelectrolyte interactions. In addition, the hydration ability of ions can also affect the counterions diffusion during the injection process, thereby affecting the liquid-liquid phase inversion. As observed in Figure 3d, the sol-gel transition time order is $t_{LiCl} > t_{NaCl} > t_{KCl}$, revealing the crosslinking process of the precursor solution injected into water (Figure 3d). The ion hydration radius (r) for Li^+ is 0.241 nm, while that for Na^+ and K^+ is 0.218 and 0.212 nm, respectively, signifying a diffusion rate order of $Li^+ < Na^+ < K^+$.[37] Despite LiCl exhibiting a lower diffusion rate compared to NaCl and KCl, its sol-gel transition time is shorter. This suggests that during the liquid-liquid phase inversion process, the viscosity of the solution plays a dominant role.

2.4. The Spreading and Wetting Performance of Injectable Hydrogel

In **Figure 4**a, the contact angles (CAs) of conventional injectable hydrogels with an entanglement state on glass in air is ≈60°. However, despite its injectability in water, the surface contact area between the hydrogel and the substrate is insignificant. This insufficiency will hinder the establishment of an interaction between the hydrogel and the substrate. In this work, we realized the complete spreading (superspreading) of injectable hydrogels on multiple surfaces underwater (schematically in Figure 4b; Figure S4, Supporting Information). The contact angles (CAs) of the QCS-CMCNa solution on polyacrylamide (PAAm) hydrogel, glass, poly (lauryl methacrylate) (PLMA) oil-gel and PTFE

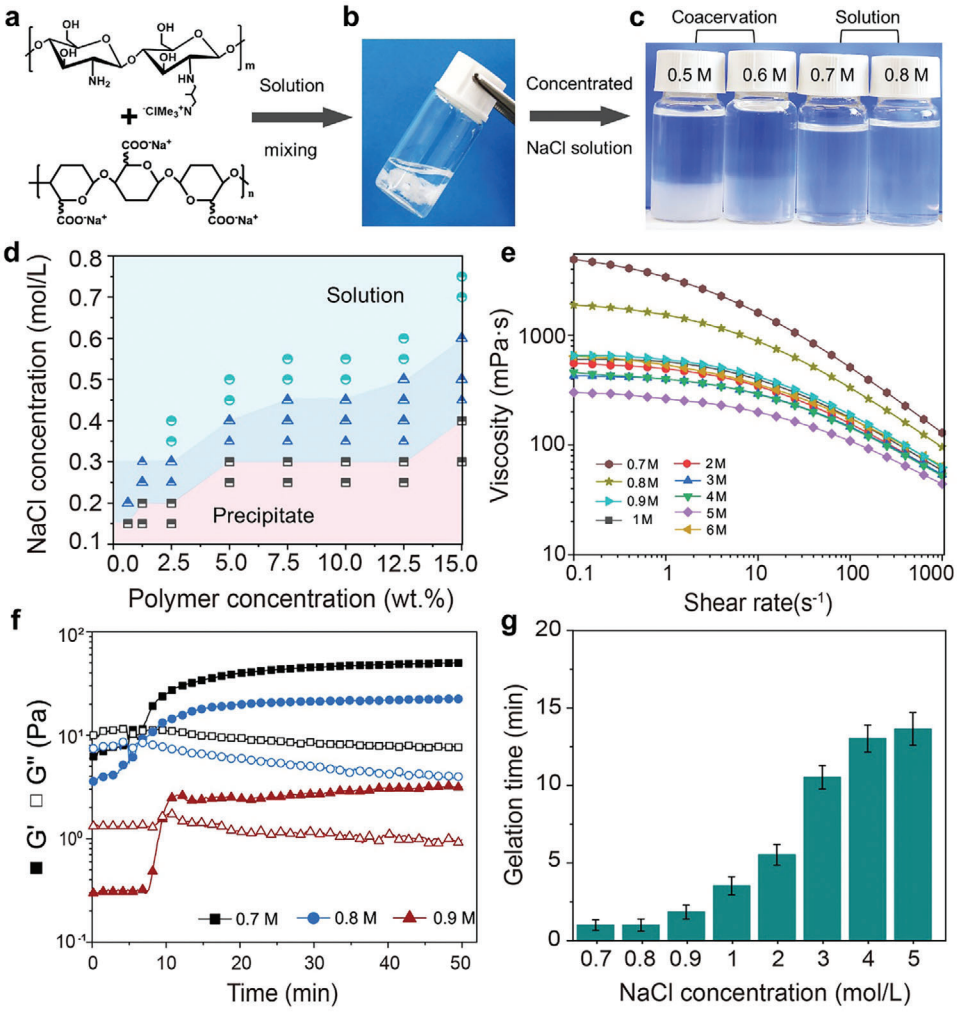

Figure 2. The chemical structures and characterization of the injectable hydrogel. a) Chemical structures of QCS and CMCNa. b) Photograph of QCS-CMCNa PECs. (c) Photographs of coacervates and solutions of QCS-CMCNa at 15 wt.% polymer concentration in the presence of 0.5, 0.6, 0.7, and 0.8 M NaCl d) Phase diagram of QCS-CMCNa polymer concentrations versus NaCl concentrations. The pink, blue, and green areas were defined as the precipitate, coacervation, and solution phases, respectively. e) The viscosity of QCS-CMCNa-15% with different NaCl concentrations. f) Dynamic time sweep rheological analysis of QCS-CMCNa-15% with different NaCl concentrations (0.7, 0.8, and 0.9 M). The crossing point of the storage modulus (G') and loss modulus (G'') was considered as the gelation time. To ensure accuracy, all measurements were repeated at least three times. g) The corresponding sol-gel transition time of QCS-CMCNa-15% at different NaCl concentrations.

surfaces in air were 10.6 ± 2.4°, 16.3 ± 2.8°, 33.1 ± 3.9° and 45.4 ± 2.3°, respectively (Figure 4c). Compared with that of water, which was 16.6 ± 2.5°, 28.6 ± 2.1°, 87.9 ± 3.3°, and 106.2 ± 2.1°, the QCS-CMCNa solution possesses a diminished contact angle with either hydrophilic or hydrophobic substrates, indicating the effective wetting and modification of substrates. They remain stable in the air and completely spread on the substrates underwater.

The superspreading process of the QCS-CMCNa solution on multiple surfaces, e.g., PAAm hydrogel, glass, PLMA oil-gel, and PTFE, in a liquid/liquid/solid system was recorded using a high-speed camera.[38] The precursor solution is injected underwater using a syringe. Upon contact with the substrate, 2 processes occur rapidly:[1] spontaneous spreading and wetting of solution on the surface, and[2] the liquid-liquid phase inversion process driven by electrostatic crosslinking (Figure S5, Supporting Information). Given their hydrophilicity, QCS-CMCNa solution enabled complete spreading and formed a hydrogel layer within 30 s on hydrophilic substrates (e.g., PAAm hydrogel and glass), and within 32 s on hydrophobic surfaces. In addition, the surfaces of hydrophilic and hydrophobic substrates become fully wetted, and underwater contact angles are nearly zero after the spreading of injectable hydrogels (Figure 4d(i–iv)).

We utilized the QCS-CMCNa solution/water/PAAm hydrogel system to analyze the spreading behavior of QCS-CMCNa-15% against PAAm hydrogel surfaces with varying NaCl concentrations. The spreading of viscous droplets on solid substrates has been extensively studied over the last decades. Many experiments and studies explore its spreading kinetics through a power law, which can be described by the relation:[39]

$$R(t) = \beta t^{n} \quad (1)$$

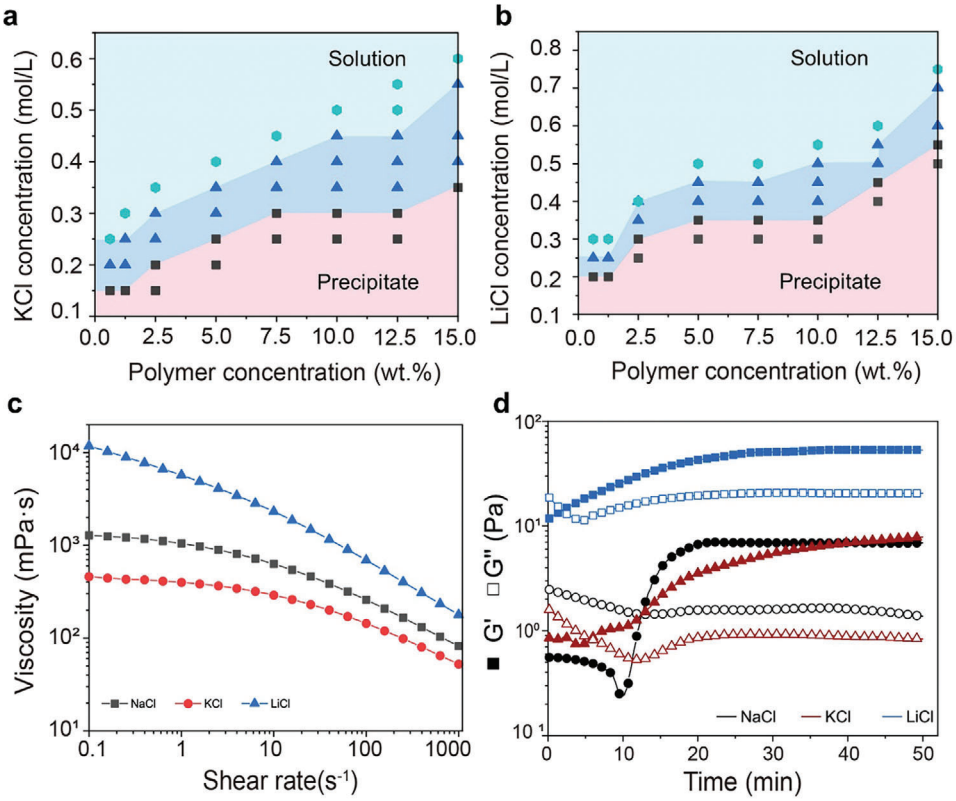

Figure 3. Phase diagram and characterization of the injectable hydrogel with KCl and LiCl. a,b) Phase diagram of QCS-CMCNa polymer concentrations versus KCl and LiCl concentrations. The pink, blue, and green areas were defined as precipitate, coacervation, and solution phases, respectively. c) The viscosity of QCS-CMCNa-15% with 4 M NaCl, KCl, and LiCl. (d) Dynamic time sweep rheological analysis of QCS-CMCNa-15% with 4 M NaCl, KCl, and LiCl. To ensure accuracy, all measurements were repeated at least three times.

where R is the spreading radius, t is the spreading time and n is the spreading exponent, which is typically described in the literature to characterize the spreading rate. According to literature reports, for droplet sizes smaller than the capillary length, the viscocapillary regime yields self-similar asymptotic dynamics, i.e., the so-called Tanner's law, with the droplet radius R increasing in time t as $\sim t^{1/10}$.[40] Ye et al. revealed that the spreading of a PDMS oil layer on flat surfaces of solutions containing anionic surfactant followed a 0.75 power law for complete wetting spreading.[41] Lee and Starov[42] revealed the difference in spreading rates between insoluble surfactant and soluble surfactant droplets on the water surface, with $t^{0.75}$ and $t^{0.5}$, respectively.

Here, we quantify the spreading dynamics of injectable hydrogels on different substrates and quantitatively compare the spreading rate by the spreading coefficient n (Table S1, Supporting Information). Take the PAAm hydrogel substrate as an example, when the salt concentration increases from 1 to 5 M, the spreading exponent becomes larger, indicating faster spreading (**Figure 5a**). This behavior correlates well with the reduced viscosity of the precursor solution upon increasing salt concentration. We have examined the spreading process of QCS-CMCNa-15% on various substrates, and similar trends have been found (Figure S6, Supporting Information). Additionally, successful superspreading relies on the compatibility of spreading liquids and substrates. The injectable hydrogel spreads faster on hydrophobic substrates, as shown in Figure 5b. In this work, injectable hydrogels not only possess high viscosity and certain compatibility with water but also are accompanied by sol-gel transition during the spreading process. These composite effects lead to a spreading exponent n ranging between 0.5 and 0.75, indicating a relatively faster rate of spreading.

The injectable hydrogel demonstrated not only super spreadability but also the capability of super wetting different surfaces, which is due to its lower interfacial tension relative to water. The spreading coefficient S is generally used to predict liquid spreading on material surfaces (Figure 5c,d).[38] Using the spreading of injectable hydrogel on the substrate under water as an example, S can be expressed as:[43]

$$\begin{aligned} S &= \gamma_{sw} - (\gamma_{hw} + \gamma_{hs}) \\ &= (\gamma_{sa} - \gamma_{aw}\cos\theta) - (\gamma_{sa} - \gamma_{ha}\cos\alpha) - \gamma_{hw} \\ &= \gamma_{ha}\cos\alpha - \gamma_{aw}\cos\theta - \gamma_{hw} \end{aligned} \quad (2)$$

where γ_{sw}, γ_{hw}, and γ_{hs} are the substrate/water, hydrogel/water, and hydrogel/substrate interfacial tensions, respectively. If S is larger than 0, then the injectable hydrogel could achieve complete wetting on substrates. As shown in Figures 4c and 5d, when the substrate is the glass, the corresponding contact angles are $\alpha \approx 16°$, $\gamma_{ha} = 70.8$ mN m^{-1} and $\theta \approx 29°$, $\gamma_{wa} = 72.3$ mN m^{-1}, respectively. Optical images of QCS-CMCNa-15% (4 M NaCl) (10 µL) in water indicate that dissolution between the two, with negligible interfacial tension makes it impossible to maintain a

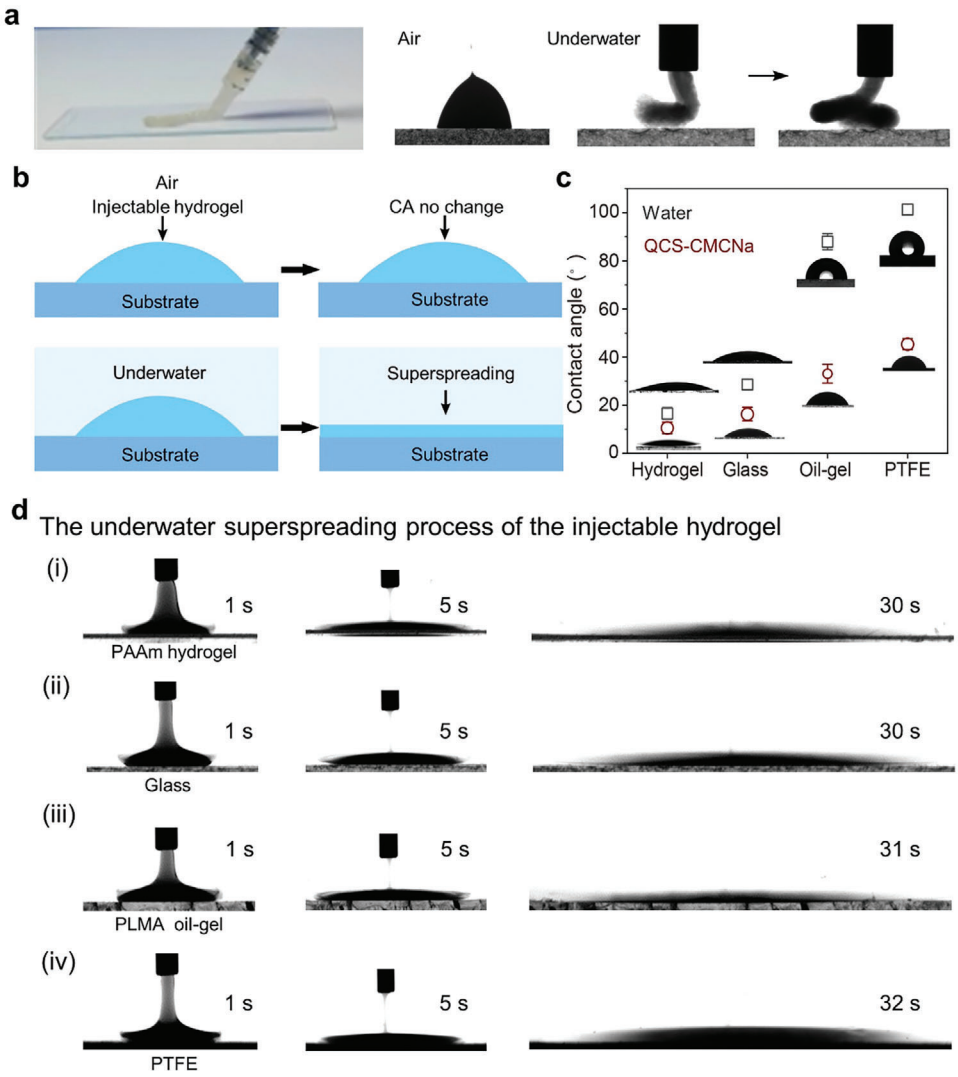

Figure 4. Spontaneous superspreading of injectable hydrogel on substrate surfaces in a liquid/liquid/solid tri-phase system. a) The injection of traditional injectable hydrogels into glass in the air and underwater. b) The contact angles of QCS-CMCNa-15% solution in air and superspreading process under water. c) The contact angles of water and QCS-CMCNa-15% solution on multiple surfaces in the air (PAAm hydrogel, glass, PLMA oil-gel, and PTFE). d) Images of the super spreading processes of QCS-CMCNa-15% solution (5 µL), which achieved complete spreading and formed a hydrogel layer on multiple surfaces (PAAm hydrogel, glass, PLMA oil-gel, and PTFE).

standard droplet (Figure S7, Supporting Information). Thus, substituting these data into Equation 1, we can obtain $S = 24.933 > 0$. Meanwhile, with the increased hydrophobicity of substrates, the large positive S favors the spreading and wetting of a liquid. Therefore, it is more conducive to the adsorption of the solution on the surface.

2.5. Preparation of the Hydrogel Coating on PDMS Substrate

We employed the super spreading property to improve the integration between the hydrogel and interface, successfully obtaining a uniform hydrogel coating on a substrate. Conventional hydrogel coating preparation methods usually inevitably contain toxic components (e.g., monomers, solvents, and initiators), which limit the application of hydrogel coatings, especially in the biomedical field.[22,44] This issue could be effectively resolved by a superspreading strategy utilizing charged biocompatible macromolecules. For instance, we successfully synthesized QCS-CMCNa hydrogel coatings with controlled thicknesses at the micro/nanoscale. 5 mL of QCS-CMCNa-15%−$_{4\,M}$ injectable hydrogel was injected onto the substrate surfaces underwater (**Figure 6a**). The fluidity of the injectable hydrogel is restricted by liquid-liquid phase inversion through electrostatic interactions, significantly improving the stability of the spreading hydrogel layer. Owing to its lower interfacial tension compared to water, the injectable hydrogel could effortlessly replace the hydration layer, completely wetting a range of material surfaces.[43] The composition and thermal stability of the hydrogel are illustrated by FT-IR and TGA cures (Figure S8, Supporting Information).

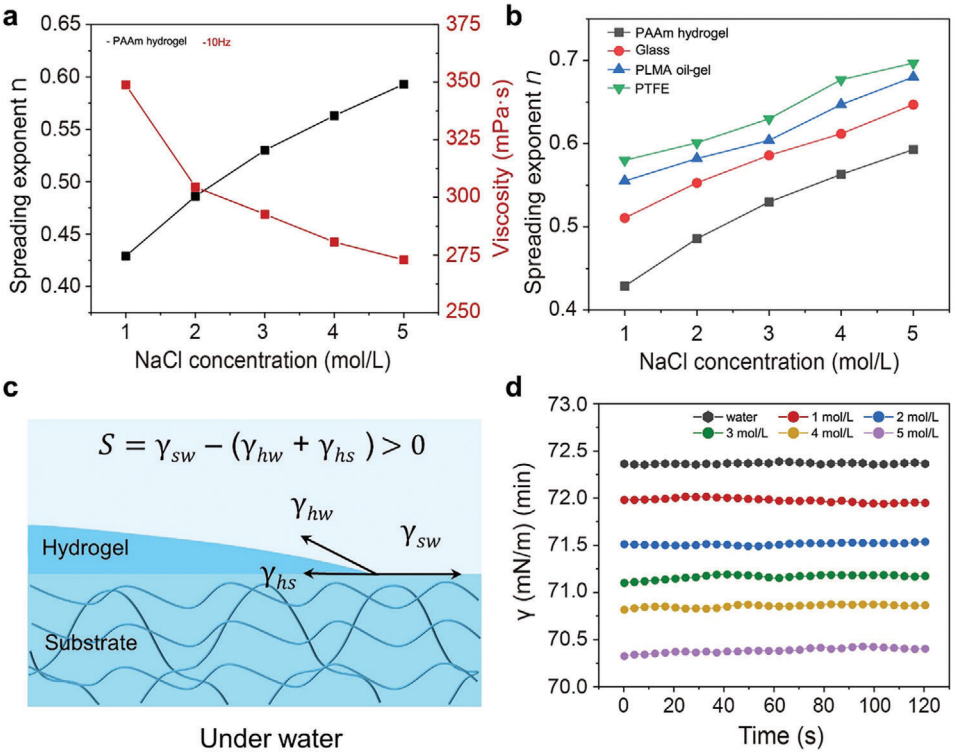

Figure 5. The superspreading performance and drive force of QCS-CMCNa-15% injectable hydrogel on substrate surfaces in a liquid/liquid/solid triphase system. a) The viscosity and spreading exponent *n* of QCS-CMCNa-15% on PAAm hydrogel substrate under different NaCl concentrations. b) The spreading exponent *n* of QCS-CMCNa-15% on substrates under different NaCl concentrations. c) Schematic diagram of the spreading coefficient *S* of injectable hydrogel spreading on substrate underwater. d) The surface tension of QCS-CMCNa-15%$-_{4\ M}$ and water in the air.

Characteristic peaks for both the QCS (1479 cm^{-1} for methyl groups of the ammonium groups) and CMCNa (1606 cm^{-1} for carbonyl groups) were found from the FT-IR spectra of the QCS-CMCNa hydrogel coating.[45,46] From their TGA curves, the initial decomposition temperature of QCS-CMCNa hydrogel coating is about 256.0 °C, whereas the initial decomposition is about 242.8 °C for QCS and 268.1 °C for CMCNa.[47] These observations confirm that the coatings are composed of QCS and CMCNa, and could be suitable for applications with temperatures below 200 °C.

We next assessed the wettability of coatings using a contact angle goniometer. As shown in Figure 6b, the contact angle of water on surfaces decreases from 50–107° to less than 10°, signifying the increased hydrophilicity of coating substrates, including glass, SiO_2, PTFE, and PDMS. Furthermore, by regulating the concentration of added salt, the coating thickness could be controlled from 4–8 µm (Figure 6c). SEM images confirmed that QCS-CMCNa coatings are fabricated with smooth and uniform surfaces. The blurry interface maintains good interfacial compatibility between the hydrogel coating and the substrate, confirming the effectiveness of the modifications (Figure 6d–f).

2.6. Performance of Hydrogel Coatings on PDMS Substrate

Microscopic observation indicated that the QCS-CMCNa coating covers the entire surface of the medical PDMS tube (**Figure** 7a). For better observation, we preadded the fluorescent dye rhodamine B to the precursor solution and showed uniform coatings under UV illumination, demonstrating the applicability of our proposed approach to complex-shaped devices.[44] Appreciable adhesion is required for most applications of hydrogel coatings which could be achieved through the covalent bonds between the hydrogel and substrate, and the energy dissipating sacrificial bonds in hydrogel.[48] Combined with two aspects: surface bridge or surface initiation method, and introducing toughenners have been reported to achieve the roust adhesion energy of ≈1300 J m^{-2}.[49] The current work focuses on the synergy effect of the superspreading and liquid-liquid phase inversion. Toughening the hydrogel bulk to realize tough hydrogel coating with strong adhesion deserves a separate project and is beyond the scope here. The stability of the coating determines the service life of medical devices. To validate the chemical stability of the hydrogel coating, we prepared a fluorescent QCS_{FITC}-CMCNa coating by labeling 20% of the added QCS with fluorescein isothiocyanate. We studied the environmental tolerance by monitoring its change of fluorescent intensity after immersing in extreme pH, high salinity, and high-temperature conditions for 24 h using confocal microscopy.[50] Moreover, we could further improve its stability through chemical crosslinking using glutaraldehyde (Figure S9, Supporting Information).[47]

To evaluate the interfacial adhesion performance of QCS-CMCNa hydrogel coating on PDMS, we performed 90° peeling tests to measure the interfacial toughness.[22,49] As shown

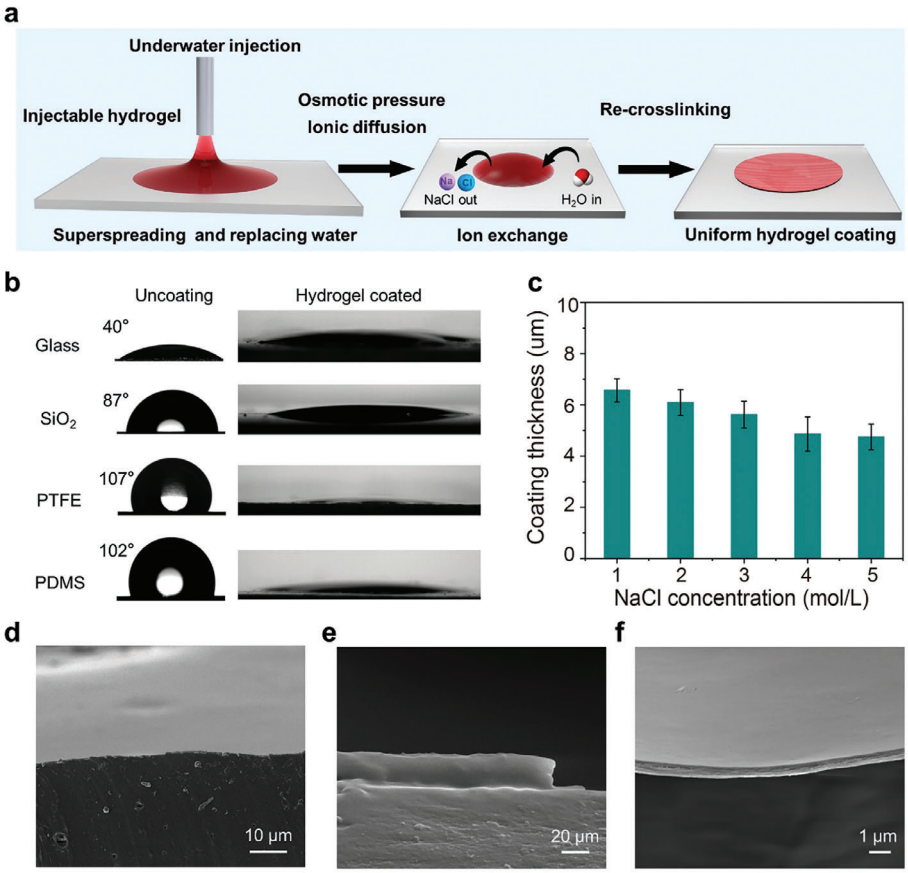

Figure 6. Hydrogel coatings of QCS-CMCNa injectable hydrogel on PDMS substrate. a) Schematic illustration of the spreading process of QCS-CMCNa injectable hydrogel on the PDMS underwater. The QCS-CMCNa injectable hydrogel was injected into water, where the NaCl diffused into water driven by osmotic pressure, leading to spreading on the substrate and liquid-liquid phase inversion, eventually forming a layer of hydrogel coating. b) The contact angle of water before and after hydrogel coating with different substrates (glass, SiO_2, PTFE, and PDMS). c) The coating thickness of the hydrogel under different salt concentrations. d–f) SEM images of the plane and cross-section of the QCS-CMCNa-15%$-_{4\ M}$ hydrogel coating on the PDMS substrate. The scale bars are 10, 20, and 1 μm.

in Figure 7b,c, the pure CMCNa and QCS films exhibit an extremely low interfacial toughness (40 and 70 J m^{-2}) and could be easily detached owing to the weak interaction between the film and the PDMS substrate, whereas a distinct adhesive failure occurs. In contrast, the QCS-CMCNa hydrogel coatings exhibit a markedly higher interfacial toughness of 455 J m^{-2} and experience failure within the QCS-CMCNa hydrogel (cohesive failure). Hence, superspreading and super-wetting properties made significant contributions to improving the interfacial performance between the hydrogel and substrates. We also investigated the lubricity of PDMS hydrogel coatings by measuring the friction coefficient (COF) using a pin-on-disk tribometer in an aqueous solution. Upon applying the QCS-CMCNa coating, the COF decreased significantly (84.3%) from 0.712 for pristine PDMS to 0.112 for the QCS-CMCNa-15%$-_{4\ M}$ hydrogel coating where physiological saline was used as a lubricant between the PTFE ball and pure PDMS (Figure 7d). As the sliding conditions increased to 2000 cycles, the COF for pure PDMS exhibited a pattern of initial increase followed by stabilization, with a notable increase of 0.732. In contrast, the hydrogel coating maintains a stable COF ≈0.116, without showing a significant increase, demonstrating the capability to withstand long-term wear and many-cycles rubbing (Figure S10, Supporting Information).[51]

According to hydration lubrication theory, a higher hydration capacity of the hydrated layer will lead to lower friction coefficients on surfaces.[52,53] In the choice of lubricative components, zwitterionic polymers have the intrinsic ability to contain more surrounding water molecules by electrostatic interactions. Zhou et al. proposed a robust polymer brush-grafted hydrogel (HHy-g-PBs) which is generated by chemically embedding hydrophilic polyanionic PSPMA brushes or the polyzwitterionic PSBMA brushes into the subsurface of the high-strength hydrogel.[51] The ultralow coefficient and excellent wear resistance performance were presented on the PBs-hydrogel composite layer, with a friction coefficient maintained at ~0.02 after 50000 friction cycles. In our research, the lubrication mechanism is related to the presence of polyelectrolytes containing both positively charged groups ($N^+(CH_3)_3$) and negatively charged groups (COO^-) in hydrogels which can be highly hydrated[54] (Figure S11, Supporting Information). Furthermore, in contrast to the marked increase in COF of pristine substrates with increasing sliding speed, the COF of hydrogel coatings demonstrated independence from friction velocity which is mainly attributed to the

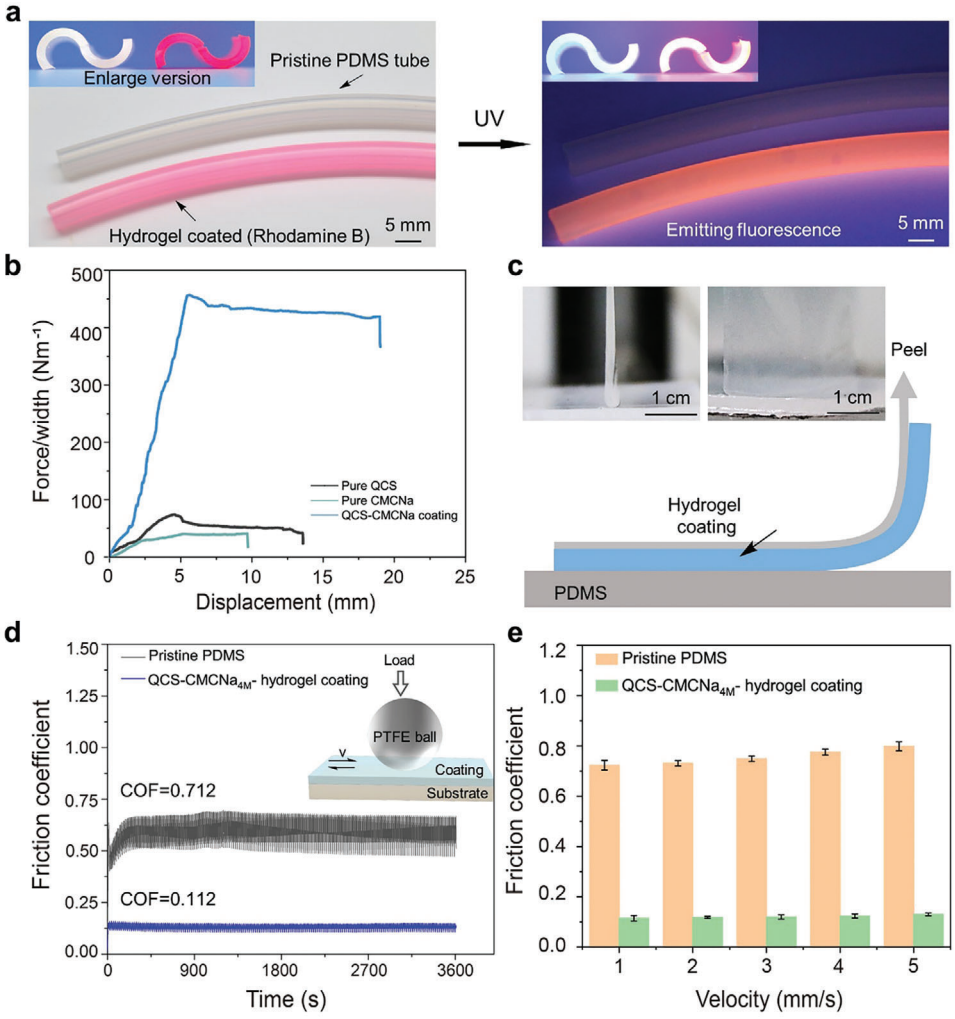

Figure 7. Macroscopic images and lubrication performance of QCS-CMCNa hydrogel coatings. a) Applicability and fluorescence images of the hydrogel coating and pristine PDMS tube. For better observation, the conformal hydrogel coating was dyed with rhodamine B. The scale bar is 5 mm. b) Representative curves of the peeling force per width (F/W) versus displacement for the QCS-CMCNa-15%–4 M hydrogel coating on a PDMS substrate, as well as pure QCS and CMCNa as a control. c) The 90-degree peel test. A hydrogel coating is peeled off at an angle of 90 degrees to the PDMS substrate. d) Comparison of lubrication performance between pristine PDMS and QCS-CMCNa hydrogel coating. The insert image is a schematic diagram of lubrication testing. The loading force was 1 N and the sliding velocity was 1 mms^{-1}. e) The lubrication performance of pristine PDMS and QCS-CMCNa hydrogel coatings at different shear velocities.

boundary lubrication mechanism of polyelectrolytes (Figure 7e). The strategy of superspreading to prepare hydrogel coating possesses the advantages of simpler, higher biocompatibility and substrate adaptability. In future research, we plan to incorporate excellent lubricative components to improve lubrication performance, which would have broader interests in the biomedical field.

3. Conclusion

To summarize, we have successfully demonstrated the effective application of superspreading and liquid-liquid phase inversion of polyelectrolyte complex solution for the fabrication of functional hydrogel coatings on diverse substrates. Upon injection of the solution underwater, counterions diffuse into water driven by osmotic pressure, leading to superspreading on the surface and rapid sol-gel transformation, ultimately producing a uniform hydrogel coating. We have extensively investigated the superspreading kinetics and the driving force of the super wetting of injectable hydrogels on various substrates. The spreading behavior is influenced by the viscosity of the solution and the diffusion of ions. The lower interfacial tension of the hydrogels allows for superwetting on different surfaces, including hydrophobic ones. The resulting coatings not only enhance the hydrophilicity, interfacial adhesion, and lubricity of the substrates but can also be further improved in terms of stability through chemical crosslinking utilizing glutaraldehyde. Our strategy provides significant potential to produce hydrogel coatings suitable for various applications. This work opens a new line of thought to investigate the behavior of superspreading and superwetting in the liquid/liquid/solid 3-phase system, which can encourage the development of conceptually novel superwettability-based chemistry and fabrication.

4. Experimental Section

Materials: Chitosan quaternary ammonium salt (QCS-98%, the viscosity of 1% aqueous solution at 20°C is 31 mPa.s, charge density, 4.5 mequiv g^{-1}) and carboxymethyl cellulose (CMCNa, the viscosity of 1% aqueous solution at 20°C is 800–1200 mPa.s, charge density, 4.6 mequiv g^{-1}) were obtained from Shanghai Macklin Biochemical Co., Ltd. Acrylamide (AAm), lauryl methacrylate (LMA, 95%, GC), N,N′-methylene bis(acrylamide) (MBAAm), ethylene glycol dimethacrylate (EGDMA, 99%), 2,2-diethoxyacetophenone (DEOP, 98%), NaCl and rhodamine B were purchased from Sigma–Aldrich and used as received. Ammonium persulfate (APS) and N,N,N′,N′-tetramethylethylenediamine (TEMED) were received from Beijing J&K Scientific Co., Ltd. Deionized water (conductivity: 0.6 μS cm^{-1}) was used in this work.

Preparation of the QCS-CMCNa Hydrogel: The QCS and CMCNa polymers were dissolved in deionized water to prepare solutions with prescribed concentrations (QCS-10 mg mL^{-1} and CMCNa-10 mg mL^{-1}). The aforementioned solutions with equal volumes were drop-blended slowly and stirred for 30 min (1000 rpm), forming compact complex precipitates. A certain amount of different concentrations of NaCl solution was added to plasticize the complex precipitates, which were stirred at 60 °C for 24 h to obtain a homogeneous solution QCS-CMCNa with the prescribed content. The QCS-CMCNa solution was injected onto substrates underwater and bulk sol-gel occurred simultaneously. After 30 s in situ conditioning without external stimuli or pressure, a layer of hydrogel appeared.

Instruments and Characterization: The spreading processes were recorded on substrates including PAAm hydrogels, glass, PLMA organogel and PTFE substrates by using a high-speed camera (i-SPEED 3, Olympus). The underwater contact angle of injectable hydrogels on a PAAm hydrogel glass, PLMA organogel and PTFE substrates were measured using a contact angle apparatus (LAUDA Scientific Surface Analyzer-LSA100) at room temperature. The morphology of obtained hydrogel coatings was characterized by scanning electronic microscopy (SEM JEOL SU8010) operated at 5 kV. The thickness of coatings was measured from the cross-sectional images taken by using SEM. The turbidity of QCS-CMCNa coacervate solutions at different salt concentrations was measured at 600 nm by UV—Vis spectrophotometry (Shimadzu UV-3600, Japan). The relative turbidity is defined as $100-100 \times 10^{-A}$ (600). Rheological measurements were carried out on an Anto Paar MCR 302 rheometer at 25 °C. The viscosity of precursor solutions was measured with a cone-shaped rotor, and the viscosity data were recorded at a range from 0.1 to 1000 s^{-1}. Time sweeps were collected in the range from 0–3000 s, 1% as the amplitude has been found to be well within the linear viscoelastic regime (LVR). Taking the QCS-CMCNa-15%$-_{4\,M}$ as an example, 0.5 mL solution was injected into the bottom steel plain plate stage (diameter, 25 mm) and maintained a hemisphere owing to its high viscosity and low surface tension. The top steel plain plate was lowered to contact the solution at a gap distance of 0.1 mm and the measurement was started. When the storage and loss modulus of the solution tended to be stable, 10 mL of water was added to the plate stage to stimulate gelation, and the data was collected from 0 s to 3000 s. To ensure accuracy, all measurements were repeated at least three times.

Supporting Information

Supporting Information is available from the Wiley Online Library or from the author.

Acknowledgements

This work was financially supported by the National Natural Science Foundation of China (No. 22341301 and 22161142021), the National Key Research and Development Program of China (No. 2022YFA1503000), and the National Natural Science Foundation of China (No. 22175010 and 22373036).

Conflict of Interest

The authors declare no conflict of interest.

Author Contributions

C.W. and M.L. conceived the idea; C.W., C.Z., Y.R., Y.S., T.Z., S.Q., J.Z., and M.L. analyzed the data and wrote the paper; C.W. performed the experiments. C.Z. and T.Z. contributed to the analysis of injectable hydrogel superspreading. Y.R. contributed to the lubrication measurements of hydrogel coatings on PDMS. Y.S. drew and optimized the figures, tables, and videos. S.Q. and J.Z. contributed to the theoretical analysis of the spreading liquid. All authors commented on the manuscript.

Data Availability Statement

The data that support the findings of this study are available from the corresponding author upon reasonable request.

Keywords

hydrogel coatings, polyelectrolyte complex solution, spreading, wetting

Received: January 10, 2024
Revised: March 22, 2024
Published online: April 9, 2024

[1] D. J. Overstreet, D. Dutta, S. E. Stabenfeldt, B. L. Vernon, *J. Polym. Sci. B Polym. Phys.* **2012**, *50*, 881.
[2] R. Dimatteo, N. J. Darling, T. I. Segura, *Adv Drug Deliv Rev.* **2018**, *127*, 167.
[3] A. Mandal, J. R. Clegg, A. C. Anselmo, S. Mitragotri, *Bioeng. Transl. Med.* **2020**, *5*, e10158.
[4] S. Correa, A. K. Grosskopf, H. Lopez Hernandez, D. Chan, A. C. Yu, L. M. Stapleton, E. A. Appel, *Chem. Rev.* **2021**, *121*, 11385.
[5] M. Liu, X. Zeng, C. Ma, H. Yi, Z. Ali, X. Mou, S. Li, Y. Deng, N. He, *Bone Res.* **2017**, *5*, 17014.
[6] D. Y. Ko, U. P. Shinde, B. Yeon, B. Jeong, *Prog. Polym. Sci.* **2013**, *38*, 672.
[7] F. Andrade, M. M. Roca-Melendres, E. F. Duran-Lara, D. Rafael, S. Schwartz Jr., *Cancers* **2021**, *13*, 1164.
[8] S. H. Hong, M. Shin, E. Park, J. H. Ryu, J. A. Burdick, H. Lee, *Adv. Funct. Mater.* **2019**, *30*, 1908497.
[9] Y. Shou, J. Zhang, S. Yan, P. Xia, P. Xu, G. Li, K. Zhang, J. Yin, *ACS Biomater. Sci. Eng.* **2020**, *6*, 3619.
[10] M. L. Pita-López, G. Fletes-Vargas, H. Espinosa-Andrews, R. Rodríguez-Rodríguez, *Eur. Polym. J.* **2021**, *145*, 110176.
[11] P. Sanchez-Cid, M. Jimenez-Rosado, A. Romero, J. F. Rubio Valle, F. J. Ostos Marcos, R.-E.-I. Benhnia, V. M. Perez-Puyana, *Polymers* **2022**, *14*, 3023.
[12] J. Hao, C. Qin, C. Wu, *Interdiscip. Mater.* **2023**, *2*, 714.
[13] Y. Li, H. Y. Yang, D. S. Lee, *J. Control Rel.* **2021**, *330*, 151.
[14] G. D. Cha, W. H. Lee, S. H. Sunwoo, D. Kang, T. Kang, K. W. Cho, M. Kim, O. K. Park, D. Jung, J. Lee, S. H. Choi, T. Hyeon, D. H. Kim, **2022**, *ACS Nano. 16*, 554.
[15] C. Cui, C. Fan, Y. Wu, M. Xiao, T. Wu, D. Zhang, X. Chen, B. Liu, Z. Xu, B. Qu, W. Liu, *Adv. Mater.* **2019**, *31*, 1905761.
[16] H. Yuk, J. Wu, T. L. Sarrafian, X. Mao, C. E. Varela, E. T. Roche, L. G. Griffiths, C. S. Nabzdyk, X. Zhao, *Nat. Biomed. Eng.* **2021**, *5*, 1131.
[17] C. Ma, J. Sun, B. Li, Y. Feng, Y. Sun, L. Xiang, B. Wu, L. Xiao, B. Liu, V. S. Petrovskii, L. Bin, J. Zhang, Z. Wang, H. Li, L. Zhang, J. Li, F.

Wang, R. Gstl, I. I. Potemkin, D. Chen, H. Zeng, H. Zhang, K. Liu, A. Herrmann, *Nat. Commun.* **2021**, *12*, 3613.
[18] J. Yang, R. Bai, B. Chen, Z. Suo, *Adv. Funct. Mater.* **2019**, *30*, 1901693.
[19] B. Su, Y. Tian, L. Jiang, *J. Am. Chem. Soc.* **2016**, *138*, 1727.
[20] J. Venzmer, *Curr. Opin. Colloid Interface Sci.* **2011**, *16*, 335.
[21] D. Parbat, N. Jana, M. Dhar, U. Manna, *ACS Appl. Mater. Interfaces* **2023**, *15*, 25232.
[22] J. Liu, S. Qu, Z. Suo, W. Yang, *Natl. Sci. Rev.* **2021**, *8*, nwaa254.
[23] Y. Yu, H. Yuk, G. A. Parada, Y. Wu, X. Liu, C. S. Nabzdyk, K. Youcef-Toumi, J. Zang, X. Zhao, *Adv. Mater.* **2019**, *31*, 1807101.
[24] J. Das, S. Mandal, A. Borbora, S. Rani, M. Tenjimbayashi, U. Manna, *Adv. Funct. Mater.* **2023**, *34*, 2311648.
[25] J. Fu, J. B. Schlenoff, *J. Am. Chem. Soc.* **2016**, *138*, 980.
[26] J. Wei, C. Zhu, Z. Zeng, F. Pan, F. Wan, L. Lei, G. Nyström, Z. Fu, *Interdiscip. Mater.* **2022**, *1*, 495.
[27] P. Schaaf, J. B. Schlenoff, *Adv. Mater.* **2015**, *27*, 2420.
[28] M. Muthukumar, *Macromolecules* **2017**, *50*, 9528.
[29] H. Dautzenberg, *Macromolecules* **1997**, *30*, 7810.
[30] V. S. Meka, M. K. G. Sing, M. R. Pichika, S. R. Nali, V. R. M. Kolapalli, P. Kesharwani, *Drug Discov. Today.* **2017**, *22*, 1697.
[31] Q. Wang, J. B. Schlenoff, *Macromolecules* **2014**, *47*, 3108.
[32] F. Luo, T. L. Sun, T. Nakajima, T. Kurokawa, A. B. Ihsan, X. Li, H. Guo, J. P. Gong, *ACS Macro Lett.* **2015**, *4*, 961.
[33] F. Zhu, L. Cheng, J. Yin, Z. L. Wu, J. Qian, J. Fu, Q. Zheng, *ACS Appl. Mater. Interfaces.* **2016**, *8*, 31304.
[34] M. Dompé, F. J. Cedano-Serrano, M. Vahdati, L. Westerveld, D. Hourdet, C. Creton, J. Gucht, T. Kodger, M. Kamperman, *Adv. Mater. Interfaces.* **2019**, *7*, 1901785.
[35] A. M. Rumyantsev, N. E. Jackson, J. J. de Pablo, *Annu. Rev. Condens. Matter Phys.* **2021**, *12*, 155.
[36] G. Liu, *Langmuir* **2019**, *35*, 3232.
[37] Y. Marcus, *J. Chem. Soc., Faraday Trans.* **1991**, *87*, 2995.
[38] P. Zhang, F. Zhang, C. Zhao, S. Wang, M. Liu, L. Jiang, *Angew. Chem. Int. Ed. Engl.* **2016**, *55*, 3615.
[39] Q. Min, Y. Y. Duan, X. D. Wang, Z. P. Liang, D. J. Lee, A. Su, *J. Colloid Interface Sci.* **2010**, *348*, 250.
[40] R. Saiseau, C. Pedersen, A. Benjana, A. Carlson, U. Delabre, T. Salez, J. P. Delville, *Nat. Commun.* **2022**, *13*, 7442.
[41] X. Ye, Y. Cheng, X.-D. Huang, H.-R. Ma, *Chin. Phys. Lett.* **2007**, *24*, 2345.
[42] K. S. Lee, V. M. Starov, *J. Colloid Interface Sci.* **2007**, *314*, 631.
[43] P. G. de Gennes, *Rev. Mod. Phys.* **1985**, *57*, 827.
[44] M. H. Bai, B. Zhao, Z. Y. Liu, Z. L. Zheng, X. Wei, L. Li, K. Li, X. Song, J. Z. Xu, Z. M. Li, **2022**, *Adv. Mater. 34*, 2108848.
[45] C. Wei, X. Zhu, H. Peng, J. Chen, F. Zhang, Q. Zhao, *ACS Sustainable Chem. Eng.* **2019**, *7*, 4508.
[46] H. Ruihua, Y. Bingchao, D. Zheng, B. Wang, *J. Mater. Sci.* **2011**, *47*, 845.
[47] J. M. Yang, W. Y. Su, T. L. Leu, M. C. Yang, *J. Membr. Sci.* **2004**, *236*, 39.
[48] X. Yao, J. Liu, C. Yang, X. Yang, J. Wei, Y. Xia, X. Gong, Z. Suo, **2019**, *Adv. Mater. 31*, 1903062.
[49] Y. Xue, X. Chen, F. Wang, J. Lin, J. Liu, *Adv. Mater.* **2023**, 2304095.
[50] H. Yu, L. Wang, Z. Zhang, X. Zhang, S. Luan, H. Shi, *Adv. Healthcare Mater.* **2023**, *12*, 2202096.
[51] M. Rong, H. Liu, M. Scaraggi, Y. Bai, L. Bao, S. Ma, Z. Ma, M. Cai, D. Dini, F. Zhou, *Adv. Funct. Mater.* **2020**, *30*, 2004062.
[52] U. Raviv, S. Giasson, N. Kampf, J.-F. Gohy, R. Jérôme, J. Klein, *Nature* **2003**, *425*, 163.
[53] J. Ahmed, T. Yamamoto, H. Guo, T. Kurokawa, T. Nonoyama, T. Nakajima, J. P. Gong, *Macromolecules* **2015**, *48*, 5394.
[54] G. Kagata, J. P. Gong, *Colloids Surf. B Biointerfaces.* **2007**, *56*, 296.